CHEMISTRY
A EUROPEAN JOURNAL

DOI: 10.1002/chem.200701419

A Heteroditopic Fluoroionophoric Platform for Constructing Fluorescent Probes with Large Dynamic Ranges for Zinc Ions

Lu Zhang, Ronald J. Clark, and Lei Zhu*[a]

Abstract: A heteroditopic fluoroionophoric platform has been designed for constructing fluorescent probes for zinc ions over large concentration ranges. The responses of the prototype probes **3a** and **3b** to zinc ions were shown to be consistent with our hypothesis, according to which the modulation of photoinduced electron transfer followed by conformation rigidification or enhanced internal charge transfer of a ditopic ligand upon successive zinc coordination affords a sensitive fluorescence enhancement in one wavelength channel followed by an emission band shift to another wavelength channel. The heteroditopic arylvinyl-bipy platform established in this study provides a lead structure for constructing fluorescent probes for real-time live cell imaging of zinc ions over broad dynamic ranges.

Keywords: analytical methods · electron transfer · fluorescence spectroscopy · photochemistry · zinc

Introduction

Sensitive and specific fluorescent probes have provided powerful means for helping unravel the biochemical roles of many vital substances.[1,2] The chemical determinant of sensitivity is the affinity of the binding moiety within a probe to the target substance. A high-affinity binding site, however, may be completely occupied at a relatively low target concentration, leading to fluorescence signal saturation. Consequently, a highly sensitive probe has a relatively narrow dynamic range centered on its dissociation constant (K_d) for the target substance,[3] rendering it ineffective in imaging substances with a large spatiotemporal flux in live cells.

Real-time imaging of the zinc ion (Zn^{2+}) in live cells[4] represents a typical challenge. Zn^{2+} is involved in numerous biochemical processes, many of which are of clinical importance.[5–8] However, the exact roles, either structural or functional, of Zn^{2+} are not entirely understood, partly because of the lack of means to determine spatiotemporal distributions of Zn^{2+} accurately in various physiological events.[9] The intracellular free (or chelatable) Zn^{2+} concentration[10] may vary from under 1 nM in the resting states of most cell types[11,12] to ≈300 μM in the synaptic vesicles in the presynaptic bouton of a neuron.[13,14] The low basal concentration and large dynamic range of physiological Zn^{2+} pose particular challenges to the development of physiological Zn^{2+} imaging technologies.

Throughout the past decade, many fluorescent Zn^{2+} probes with nanomolar or higher sensitivity have been developed for determining Zn^{2+} concentration in a physiological context.[15–20] However, the fluorescent signals of highly sensitive probes such as those in the zinquin[21–23] and zinpyr[24–32] families become saturated when Zn^{2+} concentrations are below 1 μM. Single fluorescent probes that are capable of covering the nanomolar to millimolar dynamic range of physiological Zn^{2+} are not available. Instead, combinations of probes with different affinities have been applied, with limited success, to cover large dynamic ranges.[33–36] The probe combination methods may be laborious and time-consuming, and lack accuracy, because a) parallel experiments using different probes are required, and b) different probes may have different cellular uptake rates, which impede quantitative analysis. Individual probes that are effective over the entire dynamic range of interest will be superior.

In this paper, we demonstrate a conceptually straightforward design for extending the dynamic range of fluorescent probes for Zn^{2+}. Key to the design is the incorporation of two binding sites with different affinities for Zn^{2+} into a

[a] Dr. L. Zhang, Prof. R. J. Clark, Prof. L. Zhu
Department of Chemistry and Biochemistry, Florida State University
Tallahassee, Florida 32306-4390 (USA)
Fax: (+1) 850-644-8281
E-mail: lzhu@chem.fsu.edu

Supporting information for this article (additional experimental procedures and figures) is available on the WWW under http://www.chemeurj.org/ or from the author.

probe molecule: the high-affinity site determines the sensitivity of the probe; the low-affinity site extends the dynamic range of the analysis. Non-, mono- and dicoordinated forms of the designed heteroditopic fluoroionophoric platform[37] offer three distinctive photophysical responses, which will enable the effective analysis of Zn^{2+} over relatively broad concentration ranges.

We took inspiration from reports of the application of ditopic fluorescent molecules in a sensing context. One early example, **1**, that was synthesized by the group of de Silva,[38]

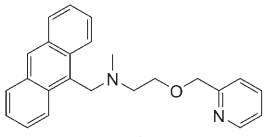

1

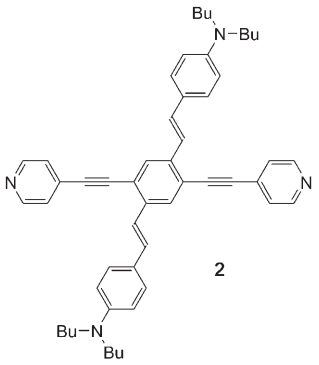

2

responds to pH changes over a wide range. At high pH (>9) **1** is not fluorescent, because of the nonradiative photoinduced electron transfer (PET) from the tertiary amino group to the anthryl excited state. The fluorescence of **1** is enhanced if the pH is low enough (≈8) to protonate the tertiary amino group, thereby terminating the PET process. If the proton concentration is high (pH<5), the pyridyl group is protonated, hence enabling PET from the anthryl excited state to the pyridinium moiety.[39] Consequently the fluorescence is quenched. Compound **1** is able to respond to proton gradients (for example, high, medium, and low) with three different photophysical states. However, the optical readouts of two states (pH high and low) are identical (fluorescence "off").

In another elegant example, Bunz's cruciform **2** shows beautiful fluorescence modulation when interacting with Zn^{2+} at different concentrations in dichloromethane.[40] In the presence of Zn^{2+}, the coordination sites on the HOMO-residing distyryl-*N*,*N*-dibutylaniline branch are occupied first, resulting in a large hypsochromic shift of the fluorescence emission. With increasing concentration of Zn^{2+}, the LUMO-residing pyridylene-ethynylene branch is also coordinated, this results in a shift of the spectrum back to a longer wavelength.[41,42] Although it is a photophysically novel system, it was not designed for effective Zn^{2+} sensing, because of the lack of Zn^{2+}-binding ligand motifs.

We aim to engineer heteroditopic fluoroionophores rationally for Zn^{2+} imaging that have the following photophysical features (Figure 1): a) the probe molecule is not fluorescent ("off") in the absence of Zn^{2+}; b) in the presence of Zn^{2+} at low concentrations, Zn^{2+} will bind to the high-affinity site to result in a sensitive concentration-dependent

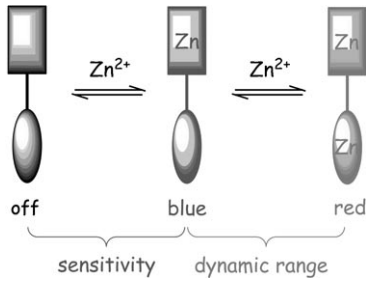

Figure 1. A fluorescent probe with two zinc binding sites (rectangle: high-affinity site; ellipse: low-affinity site). Three coordination states, non-, mono-, and dicoordinated probes are translated into three fluorescence states: off, blue, and red, respectively. The first-step coordination determines the sensitivity of Zn^{2+} detection; the second-step binding extends the dynamic range of the analysis. The color version of this figure is available in the Supporting Information.

fluorescence enhancement at a relatively short wavelength defined as the "blue" channel; c) if the Zn^{2+} concentration ($[Zn]_t$) is sufficiently high to bind to the low-affinity site, the emission band will shift to a different wavelength defined as the "red" channel. The intensity in the red channel is used to quantify $[Zn]_t$ at the high end. The changes in the blue and red channels determine the sensitivity and the dynamic range of the analysis, respectively. The two-wavelength channel (blue and red in Figure 1) strategy takes advantage of a wide span of the visible spectrum to cover a broad concentration range with high sensitivity and resolution. To the best of our knowledge, a fluorescence enhancement followed by an emission band shift of a probe molecule in response to an increase in the concentration of the target substance over a large concentration window has not been reported in the literature.

Results and Discussion

Structural platform **3** (Figure 2) was designed to achieve the coordination and photophysical objectives stipulated in Figure 1. Incorporated into platform **3** are *N*,*N*-di(2-pyridylmethyl)amino (dipicolyl) and 2,2′-bipyridyl (bipy) as the putative high- and low-affinity sites, respectively. Two monotopic model ligands **4** and **5** were used for the determination of affinities of Zn^{2+} for the respective binding motifs in **3** in aqueous solution [10 mM Hepes (4-(2-hydroxyethyl)piperazine-ethylsulfonic acid), pH 7.0, 30% dimethyl sulfoxide (DMSO)]. The association constant (K_a) of Zn^{2+} with **4** is

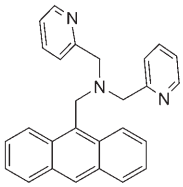

4

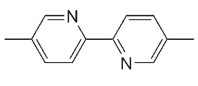

5

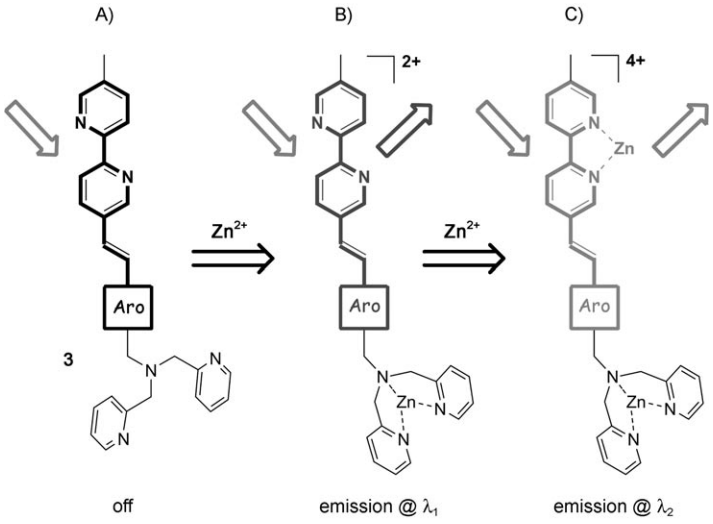

Figure 2. Designed photophysical responses of a dipicolyl-arylvinyl-bipy platform (**3**) upon coordinating one and two Zn^{2+} ions. Arrows on the left of the structures represent excitation; Arrows on the right represent emission at short B) and long C) wavelengths, respectively. Aro: aryl group. A) The fluorescence quantum yield (Φ_F) of **3** is low in the absence of Zn^{2+}; B) Φ_F increases upon coordinating the first Zn^{2+}; C) the spectrum undergoes a bathochromic shift upon binding the second Zn^{2+}. The color version of this figure is available in the Supporting Information.

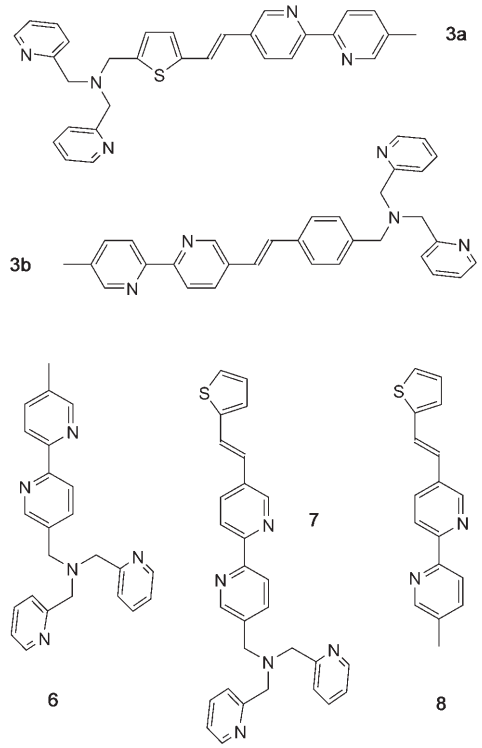

$4\times10^5\,M^{-1}$, twice that of Zn^{2+} with **5** (see the Figures S1 and S2 in the Supporting Information).

In the absence of Zn^{2+}, **3** is designed to exhibit weak fluorescence (Figure 2A) because PET from the tertiary amino group is expected to quench the excited arylvinyl-bipy fluorophore.[43] In the presence of Zn^{2+} at low concentration (for example, less than 1 equiv), preferential coordination of dipicolyl rather than bipy to Zn^{2+} occurs to stop PET, thereby increasing the fluorescence quantum yield (Φ_F) of **3** (Figure 2B).[43] Coordination with bipy to form $[Zn_2(\mathbf{3})]^{4+}$ (Figure 2C) occurs at sufficiently high $[Zn]_t$, where the bipy moiety is planarized, and the internal-charge-transferred (ICT)[44] character of the excited arylvinyl-bipy fluorophore is enhanced to result in a bathochromic shift of the emission band.[45]

The preferential binding of Zn^{2+} to the dipicolyl site is supported by the crystal structure of the monozinc(II) complex of the model ditopic compound **6** (Figure 3A). Selective binding of Zn^{2+} to the dipicolyl moiety yields a distorted trigonal-bipyramidal structure. In the unbound transoid bipyridyl moiety the two pyridyl nitrogen atoms are *anti* to each other.[46] The pyridyl rings are almost planar with a dihedral angle of 8.6°, similar to that observed in the free ligand **6** (8.2°; Figure 3B).

Compounds **3a**, **3b**, **7**, and **8** were prepared for this study: **3a** and **3b** conform to the structure **3** with Aro = thiophene and benzene, respectively. In **7**, however, the aryl and dipicolyl groups are on the opposite sides of bipy. Compound **8** represents the fluorophore of **3a**, removed from the dipicolyl group. All of the compounds undergo *trans–cis* photoisomerization under ambient irradiation. Therefore, freshly prepared solutions of *trans* compounds protected from ambient light were used for the spectroscopic studies. The isomerization occurring during a single scan is negligible.

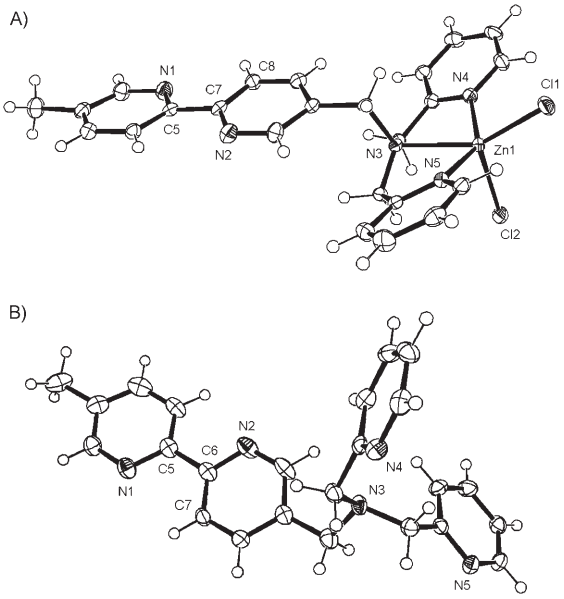

Figure 3. ORTEP diagrams (50% probability ellipsoids) of A) $[Zn(\mathbf{6})Cl_2]$. Selected bond lengths [Å] and bond angles [°]: Zn1–N4 = 2.116(3), Zn1–N5 = 2.118(3), Zn1–Cl1 = 2.2739(8), Zn1–Cl2 = 2.2885(8), Zn1–N3 = 2.309(2); N4-Zn1-N5 = 145.12(10), N4-Zn1-Cl1 = 98.16(7), N5-Zn1-Cl1 = 99.46(7), N4-Zn1-Cl2 = 103.31(8), N5-Zn1-Cl2 = 97.01(7), Cl1-Zn1-Cl2 = 113.21(3), N4-Zn1-N3 = 74.73(9), N5-Zn1-N3 = 74.45(9), Cl1-Zn1-N3 = 148.31(7), Cl2-Zn1-N3 = 98.45(6). Dihedral angle [°] N1-C5-C7-C8 = 8.65. B) Free ligand **6**, dihedral angle [°]: N1-C5-C6-C7 = 8.23.

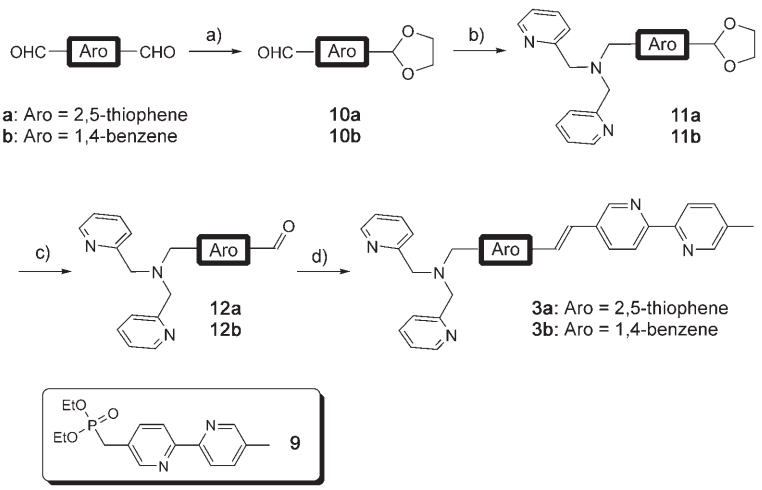

Scheme 1. Syntheses of compounds **3a** and **3b**: a) ethylene glycol, TsOH (catalyst), benzene, Dean–Stark, reflux, 4 h; b) di(2-picolyl)amine, $NaBH(OAc)_3$, RT, 6 h; c) HCl/THF/H_2O, RT, 14 h; d) NaH, dimethoxyethane, **9**, RT, 14 h.

For the rapid syntheses of **3a** and **3b** (Scheme 1), monoprotection of 2,5-thiophenedicarboxyaldehyde (**a**) and terephthalaldehyde (**b**) afforded **10a** and **10b**, respectively. The subsequent reductive amination and deprotection gave rise to **12a** and **12b**, which underwent Horner–Wadworth–Emmons reactions with phosphonate **9** to give **3a** and **3b**, respectively.

The fluorimetric titration of **3a** with Zn^{2+} in acetonitrile (MeCN) reveals two distinct coordination processes, in contrast to that of **8** (see Figure S7, in the Supporting Information), which lacks the dipicolyl group. Φ_F increases from 0.03 for **3a** alone to 0.07 in the presence of 1 equiv of Zn^{2+} (Figure 4A). A hypsochromic shift of 14 nm accompanies the enhancement. As $[Zn]_t$ exceeds 1 equiv, the emission band undergoes a bathochromic shift from $\lambda = 418$ to 496 nm (Figure 4B). This result is consistent with the hypothesis (Figure 2) that a) increasing $[Zn]_t$ to 1 equiv enhances the fluorescence of **3a** because PET ceases upon binding of Zn^{2+} to dipicolyl; b) when $[Zn]_t$ exceeds 1 equiv, the emission band undergoes a bathochromic shift, owing to planarization and/or coordination-enhanced ICT of the fluorophore upon Zn^{2+} binding at bipy.[45]

The hypsochromic emission shift of **3a** upon coordinating Zn^{2+} up to 1 equiv can be explained by analyzing the interactions between the excited-state dipole and Zn^{2+}.[40,42] The positive fluorescence solvatochromism of **8** (Figure 5) suggests that the thiophenevinyl-bipy fluorophore of **3a** has a charge-transferred excited state (Figure 6A). The electron donor, dipicolyl, is adjacent to the positive end of the excited-state dipole of **3a** (Figure 6B). The coordination of Zn^{2+} with dipicolyl creates a repulsive electrostatic interaction between the coordinated dipicolyl and the excited-state dipole (Figure 6C), which destabilizes the excited state to result in a hypsochromic shift of emission.

This explanation is supported by the photophysical behaviors of **7**, for which the electron donor dipicolyl is bonded to the negative end of the excited-state dipole instead (Figure 6D). The coordination of up to 1 equiv of Zn^{2+} to the dipicolyl in **7** provides attractive electrostatic interaction with the excited-state dipole (Figure 6E), hence giving rise to a bathochromic shift of the emission spectrum (Figure 7A). The Φ_F enhancement of **7** (Table 1) upon coordinating up to 1 equiv of $Zn^{2+}$is smaller than that of **3a**, suggesting that PET has low efficiency in the free ligand of **7**. The kinetic barrier for PET arising from the repulsive electrostatic interaction between the electron donor and the adjacent negative end of the excited-state dipole (Figure 6D) may contribute to this low PET efficiency of **7**.[47–49] The comparative study of **3a** and **7** provided guidance for positioning an electron donor in a probe molecule to achieve efficient PET.

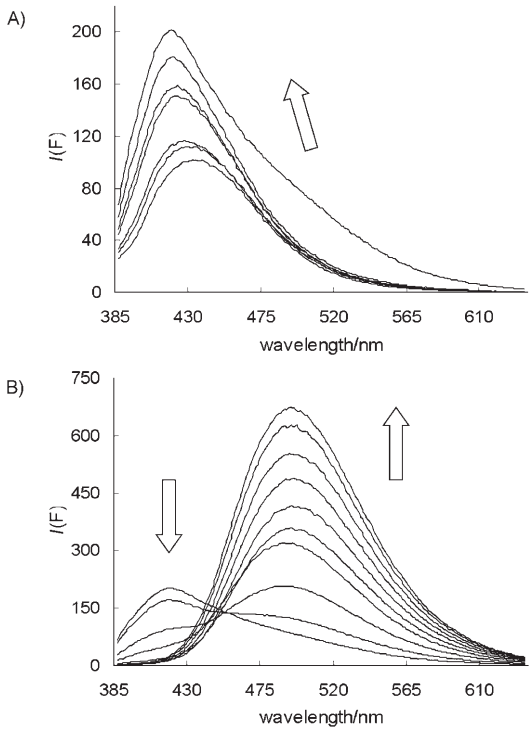

Figure 4. Fluorescence spectra ($\lambda_{ex} = 375$ nm) of **3a** (6 μM) in MeCN (TBAP: 5 mM; DIPEA: 6 μM) with incremental addition of $[Zn(OTf)_2]$ at, A) less than 6 μM and B) more than 6 μM at 25 °C. Arrows indicate the direction of spectral change with increasing $[Zn]_t$.

The viability and generality of the design in Figure 2 are demonstrated further by a photophysically improved system

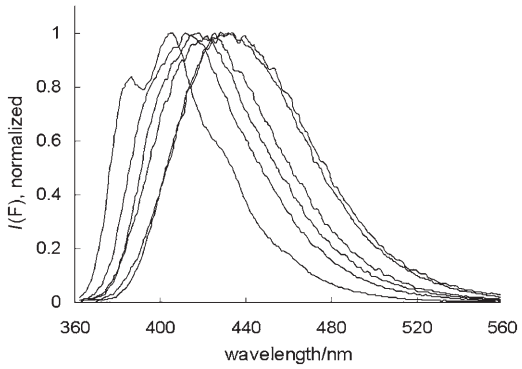

Figure 5. Normalized emission spectra of **8** in solvents of different polarity. From left to right: hexanes (dielectric constant $\varepsilon=2$); EtOAc ($\varepsilon=6$); CH_2Cl_2 ($\varepsilon=9$); MeCN ($\varepsilon=36$); DMSO ($\varepsilon=47$); MeOH ($\varepsilon=33$).

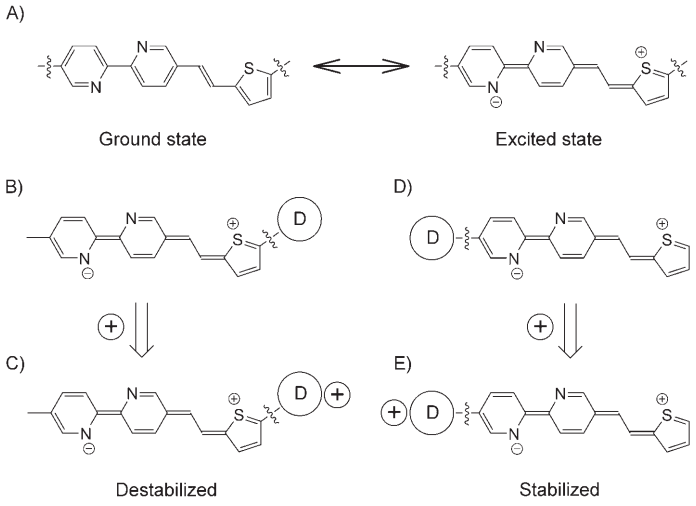

Figure 6. A) Ground- and excited-state structures of the thiophene-vinyl-bipy fluorophore; B) excited state of **3a** (D = electron-donor moiety, dipicolyl); C) coordination at the donor site destabilizes the excited state of **3a**, giving rise to a hypsochromic shift; D) excited state of **7**; E) coordination at the donor site stabilizes the excited state of **7**, affording a bathochromic shift.

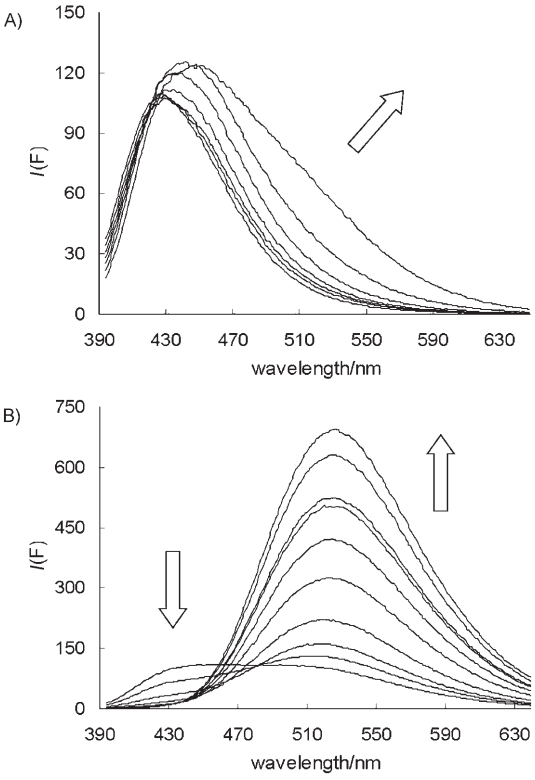

Figure 7. Fluorescence spectra of **7** (6.2 μM, $\lambda_{ex}=375$ nm) in MeCN (TBAP: 5 mM; DIPEA: 6.2 μM) upon addition of $[Zn(OTf)_2]$ (0–24 μM) at A) less than 1 equiv Zn^{2+} and B) more than 1 equiv Zn^{2+} at 25 °C. Arrows indicate the direction of spectral change with increasing $[Zn]_t$.

Table 1. Quantum yields (Φ_F) of **3a**–**b**, **7**, and **8** and their respective Zn^{II} complexes.[a]

	3a (2.8 μM)	**3b** (2.0 μM)	**7** (2.8 μM)	**8** (2.8 μM)
+0 equiv Zn^{2+}	0.03	0.03	0.04	0.04
+1 equiv Zn^{2+}	0.07	0.53	0.06	0.11
+2 equiv Zn^{2+}	0.27	0.63	0.17	0.32

[a] Fluorescence quantum yields (Φ_F) were determined in MeCN (with 1 equiv of DIPEA and 5 mM TBAP) at 25 °C by using solutions of anthracene ($\Phi_F=0.27$, ethanol), quinine sulfate ($\Phi_F=0.546$, 0.5 M H_2SO_4), and rhodamine 6G ($\Phi_F=0.95$, ethanol) as references (ref. [64]).

3b, where the extent of fluorescence enhancement upon addition of up to 1 equiv Zn^{2+} is much higher than that of **3a**. The design of **3b** was based on a thermodynamic analysis of PET. If the HOMO of the electron acceptor, which is the excited fluorophore in this study, is close to the HOMO level of the electron donor, the thermodynamic driving force of PET (ΔG_1) is small, hence reducing the PET efficiency (Figure 8A). An electron-rich fluorophore, such as that in **3a**, which contains a thiophene ring, may give rise to a high HOMO level, and therefore contribute to low PET efficiency.

Based on the above thermodynamic analysis of PET in our dipicolyl-arylvinyl-bipy system, the thiophene moiety was replaced with the less electron-rich benzene ring to afford **3b** in order to increase the thermodynamic driving force of PET ($|\Delta G_2|>|\Delta G_1|$) by reducing the HOMO of the fluorophore (Figure 8B).[50–52] As expected, the Φ_F enhancement in the presence of 1 equiv of Zn^{2+} increased from 2.3- to 18-fold (from 0.03 to 0.53; Table 1, Figure 9A). A further increase in $[Zn]_t$ results in a bathochromic shift of the emission band of **3b** (from $\lambda=395$ to 455 nm; Figure 9A). By combining the intensity data collected from the two channels at $\lambda=395$ and 455 nm, respectively (Figures 9B,C), a relatively large concentration range can be covered by a single probe.

Probe **3b** also undergoes stepwise coordination with Zn^{2+} in a neutral aqueous solution (10 mM Hepes, pH 7.0, 20% DMSO). Increasing $[Zn]_t$ results in a fluorescence enhancement followed by a bathochromic shift of the emission band (from $\lambda=410$ to 440 nm; Figure 10A). Although **3b** is a prototype probe for demonstrating the coordination and photo-

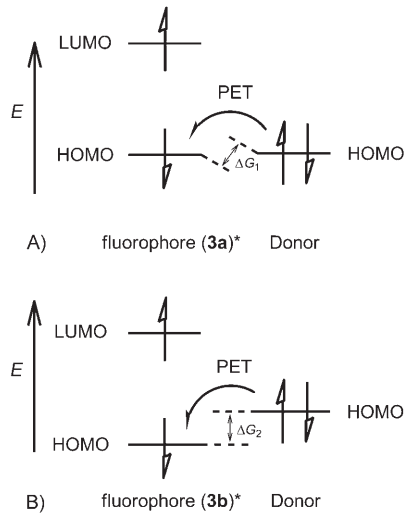

Figure 8. Modulating the thermodynamic driving forces of PET by using fluorophores with different electron densities. A) The PET driving force ΔG_1 is small in **3a**, which has an electron-rich fluorophore containing a thiophene moiety; B) $|\Delta G_2| > |\Delta G_1|$ when thiophene is replaced by the less electron-rich benzene ring in **3b**.

physical principles established in this study, the response range of **3b** to Zn^{2+} total concentration in the aqueous solution was from $<1\,\mu M$ to $>1\,mM$ (Figure 10B and Figure 10C). However, the separation observed between the two wavelength channels (30 nm) is smaller than in MeCN ($\lambda = 60$ nm), creating overlap and hence reducing the resolution between the two channels. For instance, the increase in fluorescence intensity in the blue channel (Figure 10B) at the high-concentration end resulted from the overlap between the two emission bands. Systematic structural modification of **3b** is underway for the preparation of probes with complete channel resolution (no overlap between the two emission bands) under physiological conditions.

Although metal-ion selectivity was not a particular consideration in the design of **3**, the affinities of both coordination sites in **3**, dipicolyl and bipy, to metal ions were determined separately in MeCN (Table 2) by using monotopic model compounds **4** and **5**. The association constant (K_a) of **4** with paramagnetic Cu^{2+} was determined by spectrophotometric titration. The K_a values of **4** with metal ions were determined by fluorimetric titrations, and those of **5** with metal ions by spectrophotometric titrations at low concentration of **5** ($<2\,\mu M$).

Both ligands show affinities to Zn^{2+}, Cd^{2+}, Pb^{2+}, and Cu^{2+} as expected. The titration isotherms between **4** and metal ions were fitted reasonably with a 1:1 binding equation (see the Supporting Information), consistently with reports in the literature.[53] The 2,2′-bipyridyl motif is known to form 2:1 or 3:1 complexes with transition metal ions.[54–57] However, when the concentration of **5** was kept under $2\,\mu M$, 1:1 binding[45,58] was observed for Zn^{2+}, Cu^{2+}, and Cd^{2+}, as evidenced by Job plot analysis[59] and/or fitting with a 1:1 binding equation (see the Supporting Information). On the other hand, Pb^{2+} may form polynuclear aggregates[60] with **5**

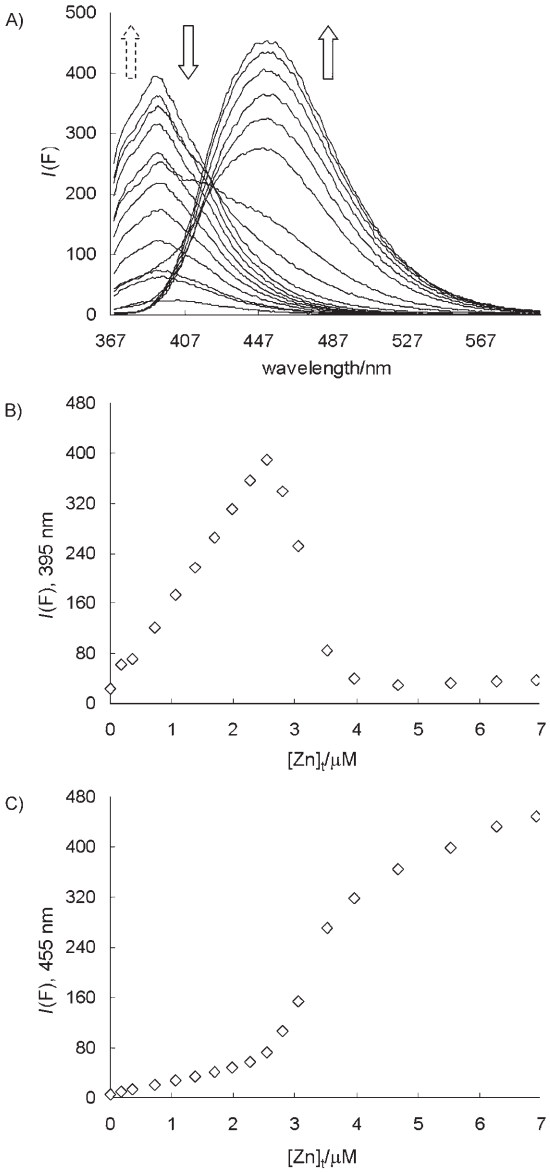

Figure 9. A) Fluorescence spectra ($\lambda_{ex} = 357$ nm) of **3b** ($2\,\mu M$) in MeCN (TBAP: 5 mM; DIPEA: $2\,\mu M$) with incremental addition of $[Zn(ClO_4)_2]$ at 25 °C. The dotted arrow indicates the direction of fluorescence enhancement as $[Zn]_t$ increases from 0 to 1.3 equiv. The solid arrows indicate the direction of the bathochromic shift as $[Zn]_t$ increases beyond 1.3 equiv. B) ,C) Fluorescence intensity observed at B) $\lambda = 395$ nm, the "blue" channel, and C) $\lambda = 455$ nm, the "red" channel.

as suggested by the Job plot analysis (see the Supporting Information).

If the metal ion concentration is high during the titration experiments in low-dielectric, organic solvents such as MeCN, there is a propensity for the formation of polynuclear complexes. For this reason we consider that the K_a values determined in MeCN are semiquantitative. Therefore, the conclusions we drew from the metal-ion titration studies using **4** and **5** are that a) the 1:1 binding affinities (K_a values) of **4** and **5** to Zn^{2+}, Cd^{2+}, Cu^{2+}, and Pb^{2+} range from 10^5 to $10^6\,M^{-1}$, if ligand concentrations are kept at the

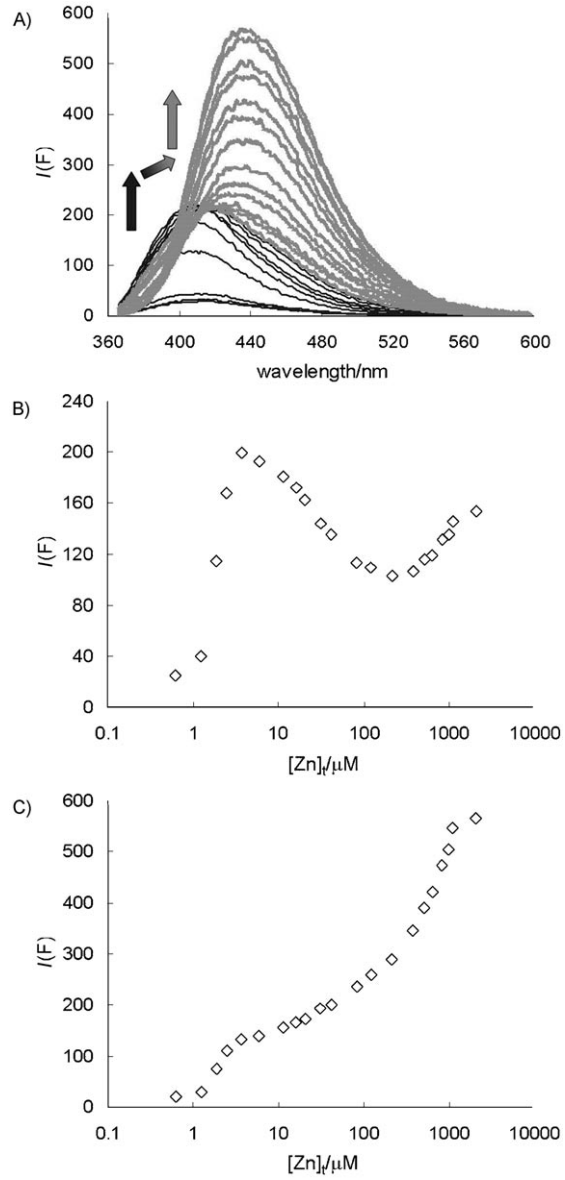

Figure 10. Fluorescence spectra of **3b** (2.0 μM, $\lambda_{ex}=352$ nm) with [Zn-$(ClO_4)_2$] (0–1035 μM) in aqueous solution (20% DMSO, 10 mM Hepes at pH 7.0) at 25 °C. A) Titration spectra. Arrows indicate the direction of spectral change with increasing $[Zn]_t$; B) fluorescence intensity at 396 nm (blue channel) vs. $[Zn]_t$ (μM); C) fluorescence intensity at $\lambda=440$ nm (red channel) vs. $[Zn]_t$ (μM).

Table 2. 1:1 association constants K_a [M^{-1}] between **4** or **5** and metal ions in MeCN.[a]

	Zn^{2+}	Cd^{2+}	Pb^{2+}	Cu^{2+}
4 (2.0 μM)	3.3×10^{6}[b]	2.4×10^{6}[b]	2.9×10^{6}[b]	1.0×10^{6}[c]
5 (1.4 μM)	7.6×10^{5}[c]	1.7×10^{6}[c]	n.d.[d]	5.5×10^{5}[c]

[a] Standard deviations of the measurements are shown in Table S1, Supporting Information. [b] K_a determined by fluorimetric titration. [c] K_a determined by spectrophotometric titration. [d] n.d.: not determined.

single-figure micromolar level; b) for a given metal ion, the affinity of **4** is always greater than the affinity of **5** in MeCN, consistent with our hypothesis.

The selectivities of **3b** toward different metal ions were also studied in aqueous solutions (10 mM Hepes, pH 7.0, 20% DMSO). The fluorescence of **3b** responds to Cd^{2+} and Zn^{2+} similarly. Pb^{2+} promotes fluorescence enhancement at low $[Pb]_t$; however, the fluorescence is quenched as $[Pb]_t$ increases further, when the bipy is probably coordinated. The fluorescence of **3b** does not change on addition of Mg^{2+} or Ca^{2+}. The paramagnetic Cu^{2+} quenches the fluorescence of **3b**, probably a result of electron transfer from the metal to the excited fluorophore.[61,62]

Conclusion

1) A heteroditopic fluoroionophoric platform has been designed rationally for constructing fluorescent probes for Zn^{2+} over large dynamic ranges. The combined power of modulation of PET and enhanced ICT upon coordination was exploited to afford a convenient analytical strategy where the probes responded to the presence of Zn^{2+} with fluorescence turn-on followed by emission band shift as $[Zn]_t$ increased over a relatively broad range.
2) We have successfully prepared and demonstrated prototype Zn^{2+}-targeting probes **3a** and **3b**. The stepwise coordination of **3a** and **3b** with Zn^{2+} was supported by X-ray crystallography using a model ditopic ligand **6**.
3) Compounds **3a** and **3b** responded to the presence of Zn^{2+} by fluorescence turn-on followed by emission band shift as designed.
4) Detailed analysis of the kinetic and thermodynamic factors pertinent to the efficiency of the PET of the probes in the absence of Zn^{2+} led to the successful rational design of **3b**.

Efforts are ongoing to construct new molecular systems for addressing sensitivity, selectivity, aqueous compatibility, and cellular uptake based on the coordination and photophysical principles established in this study.

Experimental Section

Materials and methods: Reagents and solvents were purchased from various commercial sources and used without further purification unless otherwise stated. Water used in titration experiments was deionized using the Barnstead NANOpure Diamond water system. MeCN (OmniSolv, EMD) and DMSO (ACS Reagent, >99.9%, Sigma–Aldrich) were used directly in titration experiments without purification. All reactions were carried out in oven- or flame-dried glassware in an inert Ar atmosphere. Analytical thin-layer chromatography (TLC) was performed by using pre-coated TLC plates with silica gel 60 F254 (EMD) or with aluminum oxide 60 F254 neutral (EMD). Flash column chromatography was performed by using 40–63 μm (230–400 mesh ASTM) silica gel (EMD) or alumina (80–200 mesh, pH 9–10, EMD) as the stationary phases. THF was dried by distilling from sodium/benzophenone in a continuous still under Ar protection. ^1H and ^{13}C NMR spectra were recorded at 300 and 75 MHz, respectively, by means of a Varian Mercury spectrometer. All chemical shifts were reported in δ units relative to tetramethylsilane. $CDCl_3$ was treated with alumina gel before use. High-resolution mass spectra were obtained at the Mass Spectrometry Laboratory at FSU: ESI

spectra were obtained by means of a JEOL AccuTof spectrometer, and EI spectra by using a JEOL JMS600H spectrometer. Spectrophotometric and fluorimetric titrations were conducted by using a Varian Cary 100 Bio UV–visible spectrophotometer and a Varian Cary Eclipse fluorescence spectrophotometer, respectively.

Compound 9: 5-Bromomethyl-5′-methyl-2,2′-bipyridyl[63] (0.28 mmol, 75 mg) was dissolved in triethyl phosphite (2 mL). The mixture was heated at 125 °C for 4 h. Excess of triethyl phosphite was removed under high vacuum in a fume hood. The crude product was analyzed by TLC (silica, MeOH/CH_2Cl_2 0.2 mL/4 mL, R_f = 0.35). Compound **9** was isolated by silica chromatography using 0–4 % MeOH in CH_2Cl_2 (93 %). ^{1}H NMR (300 MHz, $CDCl_3$): δ = 8.55 (s, 1 H), 8.49 (s, 1 H), 8.30 (d, J = 8.4 Hz, 1 H), 8.25 (d, J = 7.8 Hz, 1 H), 7.77 (dd, J = 2.4, 8.4 Hz, 1 H), 7.61 (dd, J = 1.8, 8.4 Hz, 1 H), 4.06 (m, 4 H), 3.18 (d, J = 21.6 Hz, 2 H), 2.38 (s, 3 H), 1.26 ppm (t, J = 7.2 Hz, 6 H).

Compound 10a: A round-bottomed flask charged with 2,5-thiophenedicarboxaldehyde (5.0 mmol, 701 mg) and ethylene glycol (5.0 mmol, 279 μL) in benzene (25 mL) was equipped with a Dean–Stark distilling receiver (5.0 mL). A catalytic amount of toluenesulfonic acid (TsOH) was added and the reaction mixture was stirred for 5 h under reflux. The reaction mixture was cooled to room temperature, then the solvent was removed and the residue was partitioned between CH_2Cl_2 and $NaHCO_3$ (0.1 M). The organic portion was separated and dried over Na_2SO_4 before the solvent was removed under vacuum. The crude product was chromatographed (silica, hexanes/CH_2Cl_2 1:1–1:9 v/v) to afford **10a** (87 %). ^{1}H NMR (300 MHz, $CDCl_3$): δ = 9.91 (s, 1 H), 7.68 (d, J = 3.6 Hz, 1 H), 7.25 (d, J = 3.6 Hz, 1 H), 6.15 (s, 1 H), 4.12 (m, 2 H), 4.08 ppm (m, 2 H); ^{13}C NMR (75 MHz, $CDCl_3$): δ = 183.35, 152.48, 143.94, 136.24, 126.82, 99.74, 65.54 ppm; HRMS (EI): m/z: calcd [M^+]: 184.0194; found: 184.0192.

Compound 10b: This was prepared by mono-protection of terephthalaldehyde with ethylene glycol, by the procedure described above for the preparation of **10a**. Yield 67 %; ^{1}H NMR (300 MHz, $CDCl_3$): δ = 10.04 (s, 1 H), 7.90 (d, J = 8.4 Hz, 2 H), 7.65 (d, J = 8.4 Hz, 2 H), 5.88 (s, 1 H), 4.16–4.04 ppm (m, 4 H).

Compound 11a: Di(2-picolyl)amine (128 mg, 1.07 mmol) was added dropwise to an anhydrous 1,2-dichloroethane (4 mL) solution of **10a** (198 mg, 1.07 mmol). The mixture was stirred overnight before $NaBH(OAc)_3$ (642 mg, 3.22 mmol) was added. The mixture was stirred for another 2 h, then the solvent was removed under vacuum. The residue was washed with basic brine (pH 11) and extracted with CH_2Cl_2 (3 × 25 mL). The organic portions were dried over K_2CO_3, and then concentrated under vacuum. Compound **11a** (163 mg, yield 41 %) was isolated by alumina chromatography (CH_2Cl_2/EtOAc, 10:1–2:1 v/v); ^{1}H NMR (300 MHz, $CDCl_3$): δ = 8.52 (d, J = 4.8 Hz, 2 H), 7.72–7.65 (m, 4 H), 7.18–7.14 (m, 2 H), 7.01 (d, J = 3.0 Hz, 1 H), 6.86 (d, J = 3.6 Hz, 1 H), 6.05 (s, 1 H), 4.19–4.00 (m, 4 H), 3.85 ppm (s, 6 H); ^{13}C NMR (75 MHz, $CDCl_3$): δ = 159.67, 149.18, 144.55, 140.89, 136.78, 126.21, 125.62, 122.94, 122.26, 100.70, 65.42, 59.95, 53.48 ppm; HRMS (ESI): m/z: calcd [M+Na^+]: 390.1252; found: 390.1250.

Compound 11b: Compound **11b** was prepared by reductive amination between **10b** and di(2-picolyl)amine, by the procedure described above for the preparation of **11a**. Yield 82 %; ^{1}H NMR (300 MHz, $CDCl_3$): δ = 8.51 (d, J = 4.2 Hz, 2 H), 7.66 (t, J = 7.8 Hz, 2 H), 7.57 (d, J = 7.8 Hz, 2 H), 7.44 (s, 4 H), 7.16–7.12 (m, 2 H), 5.79 (s, 1 H), 4.13–4.02 (m, 4 H), 3.79 (s, 4 H), 3.69 ppm (s, 2 H); ^{13}C NMR (75 MHz, $CDCl_3$): δ = 159.27, 148.61, 139.77, 136.49, 136.02, 128.44, 126.19, 122.40, 121.61, 103.21, 64.88, 59.55, 57.83 ppm; HRMS (ESI): m/z: calcd [M+Na^+]: 384.1688; found: 384.1695.

Compound 12a: Compound **11a** (173 mg, 0.47 mmol) was dissolved in a mixed solvent (14 mL) of 37 % HCl/H_2O/THF (1:6:7 by vol.). The solution was stirred overnight before being partitioned between basic brine (pH 11) and CH_2Cl_2 (3 × 25 mL). The organic portions were dried over K_2CO_3, then concentrated under vacuum. The residue was chromatographed (alumina; CH_2Cl_2/EtOAc 10:1 to 2:1 v/v) to afford **12a** (130 mg, 86 %); ^{1}H NMR (300 MHz, $CDCl_3$): δ = 9.85 (s, 1 H), 8.52 (d, J = 4.2 Hz, 2 H), 7.73–7.62 (m, 5 H), 7.19–7.17 (m, 2 H), 7.06 (d, J = 3.6 Hz, 1 H), 3.94 (s, 2 H), 3.86 ppm (s, 4 H); ^{13}C NMR (75 MHz, $CDCl_3$): δ = 183.22, 159.00, 155.79, 149.18, 143.06, 137.00, 126.71, 123.02, 122.53, 119.78, 60.01, 53.70 ppm; MS (ESI): m/z: calcd [M+Na^+]: 346.1; found: 346.1.

Compound 12b: This was prepared by deprotecting **11b** by the procedure described above for the preparation of **12a**. ^{1}H NMR (300 MHz, $CDCl_3$): δ = 9.98 (s, 1 H), 8.53 (d, J = 4.2 Hz, 2 H), 7.82 (d, J = 6.6 Hz, 2 H), 7.67 (t, J = 7.8 Hz, 2 H), 7.60–7.54 (m, 4 H), 7.18–7.14 (m, 2 H), 3.82 (s, 4 H), 3.78 ppm (s, 2 H); ^{13}C NMR (75 MHz, $CDCl_3$): δ = 191.97, 159.22, 149.11, 146.59, 136.56, 135.50, 129.86, 129.32, 122.92, 122.18, 60.17, 58.25 ppm; HRMS (ESI): m/z: calcd [M+Na^+]: 340.1426; found: 340.1421.

Compound 3a: Note: The reaction flask was protected from ambient light by aluminum foil; work-up and purification were carried out under illumination of red light bulbs. NaH (60 % in mineral oil, 26 mg, 0.66 mmol) was added to a solution of **12a** (70 mg, 0.2 mmol) in anhydrous dimethoxyethane (0.5 mL) in the reaction flask. The suspension was stirred for 8 min while the reaction mixture changed color to brown. The flask was cooled in an ice bath (0 °C) and the solution of **9** (69 mg, 0.22 mmol) in anhydrous dimethoxyethane (0.5 mL) was added dropwise. After the mixture had been stirred overnight, icy brine was added to quench the reaction. The reaction mixture was partitioned between CH_2Cl_2 and basic brine (pH 11). The organic layer was dried over Na_2SO_4, then the solvent was removed under vacuum. The residue was chromatographed on alumina gel with 10 % EtOAc in CH_2Cl_2. The isolated product (66 mg, 60 %) was precipitated from a CH_2Cl_2 solution by addition of hexanes to afford pure *trans*-**3a** (22 mg, 20 %). ^{1}H NMR (300 MHz, $CDCl_3$): δ = 8.71 (s, 1 H), 8.54 (d, J = 4.2 Hz, 2 H), 8.51 (s, 1 H), 8.34 (d, J = 8.4 Hz, 2 H), 8.29 (d, J = 8.4 Hz, 1 H), 7.91 (d, J = 8.4 Hz, 1 H), 7.73–7.62 (m, 5 H,), 7.30 (d, J = 16.2 Hz, 1 H), 7.20–7.18 (m, 2 H), 6.97–6.88 (m, 3 H), 3.89 (s, 6 H), 2.41 ppm (s, 3 H); ^{13}C NMR (75 MHz, $CDCl_3$): δ = 159.7, 155.2, 153.6, 150.0, 149.3, 148.0, 143.5, 142.1, 137.7, 136.8, 133.4, 133.2, 127.9, 127.1, 126.9, 124.3, 124.0, 123.0, 122.3, 120.9, 120.7, 60.0, 53.6, 18.6 ppm; HRMS (ESI): m/z: calcd [M+Na^+]: 512.1885; found: 512.1887.

Compound 3b: Compound **3b** was prepared by Horner–Wadworth–Emmons reaction between **12b** and **9** by the same procedure as for **3a** above. The isolated product (49.6 mg, 73 %) was precipitated from a CH_2Cl_2 solution by addition of hexanes to afford pure *trans*-**3b** (31.8 mg, 49 %). ^{1}H NMR (300 MHz, $CDCl_3$): δ = 8.74 (d, J = 1.8 Hz, 1 H), 8.55–8.51 (m, 3 H), 8.36 (d, J = 8.4 Hz, 1 H), 8.30 (d, J = 8.4 Hz, 1 H), 7.96 (dd, J = 2.4, 8.4 Hz, 1 H), 7.72–7.59 (m, 5 H), 7.52 (d, J = 8.4 Hz, 2 H), 7.44 (d, J = 8.4 Hz, 2 H), 7.24–7.08 (m, 4 H), 3.83 (s, 4 H), 3.72 (s, 2 H), 2.40 ppm (s, 3 H); ^{13}C NMR (75 MHz, $CDCl_3$): δ = 159.91, 155.27, 153.61, 149.85, 149.21, 148.19, 139.47, 137.59, 136.58, 135.87, 133.48, 132.94, 130.68, 129.51, 126.85, 124.70, 123.02, 122.15, 120.82, 120.73, 60.23, 58.46, 18.54 ppm; HRMS (ESI): m/z: calcd [M+Na^+]: 506.2321; found: 506.2312.

Example of fluorescence titration procedure: An MeCN solution of **3a** (6.0 μM), zinc trifuloromethanesulfonate [$Zn(OTf)_2$] (48.1 μM), diisopropylethylamine (DIPEA) (6.0 μM), and tetrabutylammonium perchlorate (TBAP) (5.0 mM) was titrated into a semi-micro quartz fluorimeter cuvette (Starna®) containing an MeCN solution of **3a** (840 μL, 6.0 μM), DIPEA (6.0 μM), and TBAP (5.0 mM) at 25 °C. The samples were excited at λ = 375 nm and emission spectra were collected (Figure 4).

Crystal structure determination

*Complex [Zn(**6**)Cl$_2$]*: Complex [Zn(**6**)Cl_2] was prepared by mixing an MeCN solution of $ZnCl_2$ (0.1 M, 0.2 mL) with a CH_2Cl_2 solution of **6** (0.02 M, 1.0 mL). Solvent was removed on a rotary evaporator and the crude product was washed with diethyl ether before being dried under vacuum, then redissolved in MeCN to ≈0.02 M. The solution was filtered through a Pasteur pipette plugged with glass fiber. Crystals were grown as large, colorless prisms by diffusing diethyl ether into the filtered MeCN solution of [Zn(**6**)Cl_2]. A crystal of [Zn(**6**)Cl_2] was mounted on a nylon loop and centered in the beam of 0.71073 Δ X-rays. They were indexed and found to be monoclinic. Data set were taken out to about 28° 2θ. Frame data were obtained on a Bruker SMART APEX diffractometer at T = 153 K by using a detector distance of 5 cm. The number of frames taken was 2400 with 20 second collection time followed by a final 50 frames to check on decomposition. The data sets had high redundancy

and a data/parameter ratio of more than 10:1. The integration was performed by using the SAINT program, which is part of the Bruker suite of programs. An absorption correction was done by the SADABS program and the space groups were determined by XPREP. The structure was solved by direct methods and refined by SHELXTL. The non-hydrogen atoms were refined anisotropically and then the hydrogen atoms were found by least-squares refinement with reasonable distances but were assigned as a riding model. Crystal data for $[Zn(\mathbf{6})Cl_2]$: $C_{24}H_{23}Cl_2N_5Zn$, $M_r=517.74$; crystal size $0.28\times0.12\times0.11\ mm^3$; monoclinic, $P2_1n$; $a=8.6815(7)$, $b=12.4502(11)$, $c=21.0071(18)$ Å; $\beta=92.608(2)°$; $V=2268.2$ Å^3; $Z=4$; $\rho_{calcd}=1.516\ g\,cm^{-3}$; $\mu(Mo_{K\alpha})=1.341\ mm^{-1}$; $\lambda=0.71073$ nm; $T=153(2)$ K; $2\theta_{max}=56.56°$; 30820 reflections collected; 5638 independent measured reflections; $R_1=0.0576$, $wR_2=0.1323$; residual electron density 1.153 e Å^{-3}. CCDC 657192 contains the supplementary crystallographic data for this paper. These data can be obtained free of charge from The Cambridge Crystallographic Data Centre via www.ccdc.cam.ac.uk/data_request/cif.

Compound ***6***: Crystals were grown as large, colorless needles by diffusing diethyl ether into a MeCN solution of **6**. The crystal was found to be triclinic and was solved using the method described for $[Zn(\mathbf{6})Cl_2]$. Crystal data for **6**: $C_{24}H_{23}N_5$, $M_r=381.47$; crystal size $0.60\times0.25\times0.12\ mm^3$; triclinic, $P\bar{1}$; $a=6.2393(4)$, $b=12.4910(8)$, $c=13.5777(9)$ Å; $\alpha=103.9950(10)$, $\beta=10.2550(10)$, $\gamma=95.5080(10)°$; $V=999.60(11)$ Å^3; $Z=2$; $\rho_{calcd}=1.267\ g\,cm^{-3}$; $\mu(Mo_{K\alpha})=0.078\ mm^{-1}$; $\lambda=0.71073$ nm, $T=153(2)$ K; $2\theta_{max}=56.58°$, 14109 reflections collected; 4956 independent measured reflections; $R_1=0.0808$, $wR_2=0.1628$; residual electron density 0.306 e Å^{-3}. CCDC-657193 contains the supplementary crystallographic data for this complex. These data can be obtained free of charge from the Cambridge Crystallographic Data Centre via www.ccdc.cam.ac.uk/data_request/cif.

Acknowledgement

This work was supported by Florida State University.

[1] A. P. de Silva, J. Eilers, G. Zlokarnik, *Proc. Natl. Acad. Sci. USA* **1999**, *96*, 8336.
[2] J. Zhang, R. E. Campbell, A. Y. Ting, R. Y. Tsien, *Nat. Rev. Mol. Cell Biol.* **2002**, *3*, 906.
[3] R. Haugland, in *Fluorescent and Luminescent Probes for Biological Activity* (Ed.: W. T. Mason), Academic Press, San Diego, CA, **1993**.
[4] C. J. Chang, S. J. Lippard, *Met. Ions Life Sci.* **2006**, *1*, 61.
[5] J. M. Berg, Y. Shi, *Science* **1996**, *271*, 1081.
[6] A. I. Bush, *Curr. Opin. Chem. Biol.* **2000**, *4*, 184.
[7] W. Maret, *BioMetals* **2001**, *14*, 187.
[8] C. J. Frederickson, A. I. Bush, *BioMetals* **2001**, *14*, 353.
[9] A. R. Kay, *Trends Neurosci.* **2006**, *29*, 200.
[10] L. A. Finney, T. V. O'Halloran, *Science* **2003**, *300*, 931.
[11] A. Krezel, W. Maret, *J. Biol. Inorg. Chem.* **2006**, *11*, 1049.
[12] C. E. Outten, T. V. O'Halloran, *Science* **2001**, *292*, 2488.
[13] S. Y. Assaf, S.-H. Chung, *Nature* **1984**, *308*, 734.
[14] C. J. Frederickson, J.-Y. Koh, A. I. Bush, *Nat. Rev. Neurosci.* **2005**, *6*, 449.
[15] E. Kimura, T. Kioke, *Chem. Soc. Rev.* **1998**, *27*, 179.
[16] S. C. Burdette, S. J. Lippard, *Proc. Natl. Acad. Sci. USA* **2003**, *100*, 3605.
[17] K. Kikuchi, H. Komatsu, T. Nagano, *Curr. Opin. Chem. Biol.* **2004**, *8*, 182.
[18] P. Jiang, Z. Guo, *Coord. Chem. Rev.* **2004**, *248*, 205.
[19] N. C. Lim, H. C. Freake, C. Bruckner, *Chem. Eur. J.* **2005**, *11*, 38.
[20] P. Carol, S. Sreejith, A. Ajayaghosh, *Chem. Asian J.* **2007**, *2*, 338.
[21] C. J. Frederickson, E. J. Kasarskis, D. Ringo, R. E. Frederickson, *J. Neurosci. Methods* **1987**, *20*, 91.
[22] C. J. Fahrni, T. V. O'Halloran, *J. Am. Chem. Soc.* **1999**, *121*, 11448.
[23] M. S. Nasir, C. J. Fahrni, D. A. Suhy, K. J. Kolodsick, C. P. Singer, T. V. O'Halloran, *J. Biol. Inorg. Chem.* **1999**, *4*, 775.
[24] G. K. Walkup, S. C. Burdette, S. J. Lippard, R. Y. Tsien, *J. Am. Chem. Soc.* **2000**, *122*, 5644.
[25] S. C. Burdette, G. K. Walkup, B. Spingler, R. Y. Tsien, S. J. Lippard, *J. Am. Chem. Soc.* **2001**, *123*, 7831.
[26] S. C. Burdette, S. J. Lippard, *Inorg. Chem.* **2002**, *41*, 6816.
[27] S. C. Burdette, C. J. Frederickson, W. Bu, S. J. Lippard, *J. Am. Chem. Soc.* **2003**, *125*, 1778.
[28] C. C. Woodroofe, S. J. Lippard, *J. Am. Chem. Soc.* **2003**, *125*, 11458.
[29] C. J. Chang, J. Jaworski, E. M. Nolan, M. Sheng, S. J. Lippard, *Proc. Natl. Acad. Sci. USA* **2004**, *101*, 1129.
[30] E. M. Nolan, S. C. Burdette, J. H. Harvey, S. A. Hilderbrand, S. J. Lippard, *Inorg. Chem.* **2004**, *43*, 2624.
[31] C. C. Woodroofe, R. Masalha, K. R. Barnes, C. J. Frederickson, S. J. Lippard, *Chem. Biol.* **2004**, *11*, 1659.
[32] C. C. Woodroofe, A. C. Won, S. J. Lippard, *Inorg. Chem.* **2005**, *44*, 3112.
[33] E. M. Nolan, J. Jaworski, K.-I. Okamoto, Y. Hayashi, M. Sheng, S. J. Lippard, *J. Am. Chem. Soc.* **2005**, *127*, 16812.
[34] M. D. Shults, D. A. Pearce, B. Imperiali, *J. Am. Chem. Soc.* **2003**, *125*, 10591.
[35] K. Komatsu, K. Kikuchi, H. Kojima, Y. Urano, T. Nagano, *J. Am. Chem. Soc.* **2005**, *127*, 10197.
[36] C. R. Goldsmith, S. J. Lippard, *Inorg. Chem.* **2006**, *45*, 555.
[37] H.-G. Lohr, F. Vogtle, *Acc. Chem. Res.* **1985**, *18*, 65.
[38] A. P. de Silva, H. Q. N. Gunaratne, C. P. McCoy, *Chem. Commun.* **1996**, 2399.
[39] A. P. de Silva, H. Q. N. Gunaratne, P. L. M. Lynch, *J. Chem. Soc. Perkin Trans. 2* **1995**, 685.
[40] J. N. Wilson, U. H. F. Bunz, *J. Am. Chem. Soc.* **2005**, *127*, 4124.
[41] J. N. Wilson, M. Josowicz, Y. Wang, U. H. F. Bunz, *Chem. Commun.* **2003**, 2962.
[42] A. J. Zucchero, J. N. Wilson, U. H. F. Bunz, *J. Am. Chem. Soc.* **2006**, *128*, 11872.
[43] A. P. de Silva, H. Q. N. Gunaratne, T. Gunnlaugsson, A. J. M. Huxley, C. P. McCoy, J. T. Rademacher, T. E. Rice, *Chem. Rev.* **1997**, *97*, 1515.
[44] B. Valeur, I. Leray, *Coord. Chem. Rev.* **2000**, *205*, 3.
[45] A. Ajayaghosh, P. Carol, S. Sreejith, *J. Am. Chem. Soc.* **2005**, *127*, 14962.
[46] G. S. Hanan, J.-M. Lehn, N. Kyritsakas, J. Fischer, *J. Chem. Soc. Chem. Commun.* **1995**, 765.
[47] A. P. de Silva, H. Q. N. Gunaratne, J.-L. Habib-Jiwan, C. P. McCoy, T. E. Rice, J.-P. Soumillion, *Angew. Chem.* **1995**, *107*, 1889; *Angew. Chem. Int. Ed. Engl.* **1995**, *34*, 1728.
[48] N. C. Lim, C. Bruckner, *Chem. Commun.* **2004**, 1094.
[49] N. A. O'Connor, S. T. Sakata, H. Zhu, K. J. Shea, *Org. Lett.* **2006**, *8*, 1581.
[50] K. Tanaka, T. Miura, N. Umezawa, Y. Urano, K. Kikuchi, T. Higuchi, T. Nagano, *J. Am. Chem. Soc.* **2001**, *123*, 2530.
[51] T. Ueno, Y. Urano, K.-i. Setsukinai, H. Takakusa, H. Kojima, K. Kikuchi, K. Ohkubo, S. Fukuzumi, T. Nagano, *J. Am. Chem. Soc.* **2004**, *126*, 14079.
[52] E. Kawabata, K. Kikuchi, Y. Urano, H. Kojima, A. Odani, T. Nagano, *J. Am. Chem. Soc.* **2005**, *127*, 818.
[53] S. A. de Silva, A. Zavaleta, D. E. Baron, O. Allam, E. V. Isidor, N. Kashimura, J. M. Percapio, *Tetrahedron Lett.* **1997**, *38*, 2237.
[54] A. Bilyk, M. M. Harding, P. Turner, T. W. Hambley, *J. Chem. Soc. Dalton Trans.* **1994**, 2783.
[55] B. Murphy, M. Aljabri, M. Light, M. B. Hursthouse, *J. Chem. Crystallogr.* **2003**, *33*, 195.
[56] M. S. Juric, P. Planinic, G. Giester, *Acta Crystallogr. Sect. A* **2006**, *E62*, m2826.
[57] P. Lemoine, K. Bendada, B. Viossat, *Acta Crystallogr. Sect. A* **2004**, *C60*, m489.
[58] B. Turfan, E. U. Akkaya, *Org. Lett.* **2002**, *4*, 2857.
[59] Based on Job plot analysis, the coordination stoichiometry between Zn^{2+} and **5** shifts from 2:1 to 1:1 as the concentration of **5** decreases (see the Supporting Information).
[60] B. Wang, M. R. Wasielewski, *J. Am. Chem. Soc.* **1997**, *119*, 12.

[61] E. U. Akkaya, M. E. Huston, A. W. Czarnik, *J. Am. Chem. Soc.* **1990**, *112*, 3590.
[62] R. Kraemer, *Angew. Chem.* **1998**, *110*, 804; *Angew. Chem. Int. Ed.* **1998**, *37*, 772.
[63] R. Heck, F. Dumarcay, A. Marsura, *Chem. Eur. J.* **2002**, *8*, 2438.
[64] S. Fery-Forgues, D. Lavabre, *J. Chem. Educ.* **1999**, *76*, 1260.

Received: September 7, 2007
Published online: January 29, 2008

